Non-singular Terminal Sliding Mode Compliance Control of Aerial Manipulator Based on Disturbance Observer

WEN Zunwang, WANG Yaoyao, FU Hao, TAN Rongkai, WANG Ning*

College of Mechanical and Electrical Engineering, Nanjing University of Aeronautics and Astronautics, Nanjing 210016, P.R. China

(Received 2 August 2023; revised 29 August 2023; accepted 2 September 2023)

Abstract: Aiming at the contact operation problem of aerial manipulator, a non-singular terminal sliding mode compliant control algorithm for aerial manipulator based on disturbance observer is designed. The algorithm introduces disturbance observer on the basis of nonsingular terminal sliding mode control. The disturbance is estimated to reduce the system estimation error, the disturbance of the manipulator and the influence of external disturbance on the rotorcraft. Finally, the simulation results show that the proposed controller has good robustness. Meanwhile, it can reduce the system estimation error, the disturbance of the manipulator and the external disturbance, and ensure the stability of the contact force under smooth movement.

Key words: aerial manipulator; disturbance observer; terminal sliding mode; admittance control

CLC number: TP249 **Document code:** A **Article ID:** 1005-1120(2023)S2-0069-08

0 Introduction

The aerial manipulator combines the aerial motion of the rotorcraft with the maneuverability of the manipulator, and such an aircraft has the potential for flexible operation in complex environments, rather than just for simple observation[1]. According to the characteristics of interaction with the environment during operation, the operation tasks of the aerial manipulator can be divided into free flight operations[2] and motion restricted operations[3]. In the process of restricted motion operations, it is usually necessary to contact the external environment for a long time. The introduction of compliance control for such operations will greatly improve the operation efficiency and ensure the safety of the operation. However, there are some difficulties that restrict the compliant control of the flying manipulator. First, the load capacity of ordinary rotorcraft is small, and the load capacity of the installation operation device is further reduced, thereby increasing the difficulty of control. Second, the flying manipulator is a rootless system, and the disturbance of the environment further increases the disturbance to the rotorcraft. Third, due to the pose error, the contact force may be too large, which affects the safety and efficiency of the work.

In order to improve the flexibility of air contact operations, researchers have made many achievements. Bellens et al.[4] proposed a hybrid attitude/torque control framework for a quadrotor, which made the quadrotor in direct contact with the environment and moved stably upon contact. James et al.[5] introduced the physical coupling between the flying manipulator and the tree and a new application in canopy sampling, using the unmanned aerial vehicle (UAV) dynamic modeling method and the branch mechanical model to introduce the drone-branch interaction model to study the environmental interference of UAVs. Ref.[6] studied the use of a flying robotic arm to open and close an unknown drawer. A multi-rotor was combined with a robotic arm for

*Corresponding author, E-mail address: yywang_cmee@nuaa.edu.cn.

How to cite this article: WEN Zunwang, WANG Yaoyao, FU Hao, et al. Non-singular terminal sliding mode compliance control of aerial manipulator based on disturbance observer[J]. Transactions of Nanjing University of Aeronautics and Astronautics, 2023, 40(S2): 69-76.

http://dx.doi.org/10.16356/j.1005-1120.2023.S2.010

operational tasks. Their method was validated experimentally, including opening and closing a drawer, which validated the effectiveness of the method. Takahiro et al.[7] introduced an octa-rotor UAV for bridge inspection with a single degree of freedom (DoF) manipulator, which has the ability to contact bridge piers for contact testing. Contact experiments showed that the UAV could control the contact force between its end effector and the bridge pier. The average error in contact force was 4.27 ± 3.64 N relative to the force required for 20 N. Caccavale et al.[8] proposed an impedance control scheme with flying manipulator cooperating to limit the contact force due to object/environment interaction and the internal force due to manipulator/object interaction, which was verified by simulation of the effectiveness of the method.

To target these short comings mentioned above, this paper designs a non-singular terminal sliding mode compliance controller based on disturbance observer to ensure the compliance control between the aerial manipulator and the outside. It can reduce the estimation error of the system. The disturbance is estimated to reduce the system estimation error, the disturbance of the manipulator and the influence of external disturbance on the rotorcraft. It improves the stability of the contact force and the flexibility of air contact operations. In this paper, the kinematics and dynamics of the aerial manipulator are modeled. Then, the controller is designed and its stability is analyzed, and the controller of the rotorcraft and the compliance controller of the manipulator are designed. Finally, in order to verify the proposed control algorithm, a simulation comparison experiment is carried out.

1 System Design and Dynamic Modeling of Aerial Manipulator

1.1 Structure design of aerial manipulator

The aerial manipulator designed in this paper is composed of a quadrotor rotorcraft and a manipulator, as shown in Fig.1. The total mass of the aerial manipulator is about 2.4 kg, of which the rotorcraft wheelbase is 550 mm, and the mass of the rotorcraft is about 2 kg. The manipulator adopts a cable-driven manipulator, and the motor is placed at the base and connected by the cable drive, so as to reduce the disturbance to the body. The manipulator has a total of two degrees of freedom and a length of 350 mm, of which the movable arm part is 400 g.

Fig.1 Structure of aerial manipulator

1.2 Dynamic model of rotorcraft

The coordinate system of the aerial manipulator is shown in Fig.2. The coordinate system consists of three parts: The ground coordinate system O_g, the coordinate system O_a fixed to the center of the rotorcraft, and the end coordinate system O_e of the manipulator.

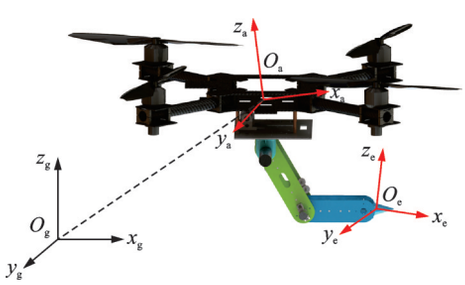

Fig.2 Reference frames for an aerial manipulator

The relationship between the coordinate systems can be expressed by the rotation matrix. It is assumed that the attitude angle of the rotorcraft is $\boldsymbol{\Phi} = [\varphi \ \theta \ \psi]$, which corresponds to the roll angle, pitch angle and yaw angle of the UAV in turn. The rotation matrix can be calculated from the transformation matrices R_x, R_y, R_z

$$\boldsymbol{R}_b = R_x R_y R_z = \begin{bmatrix} \cos\psi\cos\theta & \sin\varphi\sin\theta\cos\psi - \sin\psi\cos\varphi & \sin\psi\sin\varphi + \cos\psi\sin\theta\cos\varphi \\ \sin\psi\cos\theta & \cos\psi\cos\varphi + \sin\psi\sin\theta\sin\varphi & \sin\psi\sin\theta\cos\varphi - \cos\psi\sin\varphi \\ -\sin\theta & \cos\theta\sin\varphi & \cos\theta\cos\varphi \end{bmatrix} \tag{1}$$

where the pitch and roll angles are within 90 °. According to the rotation matrix, the dynamic model of rotorcraft can be obtained

$$\begin{cases} m\ddot{x} = u_1(\cos\psi\sin\theta\cos\varphi + \sin\psi\sin\varphi) - k_x\dot{x} + f_x \\ m\ddot{y} = u_1(\sin\psi\sin\theta\cos\varphi - \cos\psi\sin\varphi) - k_y\dot{y} + f_y \\ m\ddot{z} = u_1\cos\varphi\cos\theta - k_z\dot{z} + f_z - mg \\ I_x\ddot{\varphi} = u_2 + \dot{\theta}\dot{\psi}(I_y - I_z) - k_\varphi\dot{\varphi} + \tau_\varphi \\ I_y\ddot{\theta} = u_3 + \dot{\varphi}\dot{\psi}(I_y - I_z) - k_\theta\dot{\theta} + \tau_\theta \\ I_z\ddot{\psi} = u_4 + \dot{\theta}\dot{\varphi}(I_y - I_z) - k_\psi\dot{\psi} + \tau_\psi \end{cases} \tag{2}$$

where f and τ are the external force of the rotorcraft, which are composed of three parts: The first part is the disturbance of the manipulator to the rotorcraft, and it will be calculated in the next part, including the disturbance caused by the manipulator itself and the disturbance of the contact force; the second part is the disturbance caused by the time-varying dynamic parameters of the rotorcraft, which may be caused by inaccurate parameter estimation; the third part is other unknown disturbances to the rotorcraft. The calculation method of $[\ u_1 \quad u_2 \quad u_3 \quad u_4\ ]^{\mathrm{T}}$ is as follows

$$\begin{bmatrix} u_1 \\ u_2 \\ u_3 \\ u_4 \end{bmatrix} = \begin{bmatrix} c_f & c_f & c_f & c_f \\ \frac{\sqrt{2}}{2}\mathrm{d}c_f & -\frac{\sqrt{2}}{2}\mathrm{d}c_f & -\frac{\sqrt{2}}{2}\mathrm{d}c_f & \frac{\sqrt{2}}{2}\mathrm{d}c_f \\ \frac{\sqrt{2}}{2}\mathrm{d}c_f & \frac{\sqrt{2}}{2}\mathrm{d}c_f & -\frac{\sqrt{2}}{2}\mathrm{d}c_f & -\frac{\sqrt{2}}{2}\mathrm{d}c_f \\ c_M & -c_M & c_M & -c_M \end{bmatrix} \begin{bmatrix} \omega_1^2 \\ \omega_2^2 \\ \omega_3^2 \\ \omega_4^2 \end{bmatrix} \tag{3}$$

where c_f and c_M are the lift coefficient and torque coefficient of the propeller, respectively.

1.3 Dynamic model of manipulator

The calculation method of the disturbance of the manipulator to the UAV can be calculated by Newton-Euler iterative method. The calculation process includes two steps: First, the velocity and acceleration of the connecting rod are calculated by the outward iteration method; second, the force and moment are calculated by the inward iteration method. The calculated force and moment of the first joint are the disturbance to the rotorcraft.

The method of calculating the centroid velocity and acceleration of the connecting rod by the outward iteration method is

$$\begin{cases} {}^{i+1}\omega_{i+1} = {}_i^{i+1}R\,{}^i\omega_i + \dot{\theta}_{i+1}\,{}^{i+1}\hat{Z}_{i+1} \\ {}^{i+1}v_{i+1} = {}_i^{i+1}R({}^iw_i \times {}^iP_{i+1} + {}^iw_i \times ({}^iw_i \times {}^iP_{i+1})) + {}^i\dot{v}_i \end{cases} \tag{4}$$

After calculating the velocity and acceleration of the center of mass of all links, the inertia force and moment acting on the center of mass of links are calculated by the Newton Euler formula

$$\begin{cases} F_i = m\dot{v} \\ N_i = I\dot{\omega}_i + \omega_i I\omega_i \end{cases} \tag{5}$$

According to the above calculated force and torque, the joint torque, list the force and torque balance are calculated as

$$\begin{cases} {}^if_i = {}_{i+1}^iR\,{}^{i+1}f_{i+1} + {}^iF_i \\ {}^in_i = {}^iN_i + {}_{i+1}^iR\,{}^{i+1}n_{i+1} + {}^iP_{C_i} \times {}^iF_i + {}^iP_{i+1} \times {}_{i+1}^iR\,{}^{i+1}f_{i+1} \end{cases} \tag{6}$$

Based on Eq.(6), the disturbance of the robotic arm to the rotorcraft is calculated.

1.4 Contact force model of aerial manipulator

In the contact operation, due to the positioning error of the aerial manipulator and the environment or the uncertainty of the model, it may have a great contact force with the environment, resulting in instability or even destruction of the system. Therefore, compliant control is needed. The design idea is to make the end of the manipulator show the characteristics of spring-mass-damping. In order to achieve compliance control, the contact force model of the aerial manipulator needs to be analyzed first.

As shown in Fig.3, the end of the manipulator contacts the plane, and the interaction force can be decomposed into three directions. The force perpendicular to the plane shows the characteristics of spring-mass-damping, and the other two directions

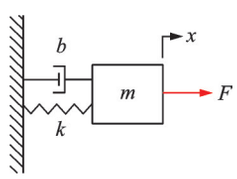

Fig.3 Spring-mass-damper model

are mainly subjected to friction. The calculation of the force F perpendicular to the plane and the calculation of the friction force are

$$\begin{cases} F_z = k_d(x_r - x) + b_d(\dot{x}_r - \dot{x}) + m_d(\ddot{x}_r - \ddot{x}) \\ F_x = -\operatorname{sign}(v_x)\mu F_z \dfrac{v_x}{v} \\ F_y = -\operatorname{sign}(v_y)\mu F_z \dfrac{v_y}{v} \\ v = \sqrt{v_x^2 + v_y^2} \end{cases} \tag{7}$$

when v is greater than 0.01 m/s. According to the above calculation, when v is less than 0.01 m/s, it can be approximately considered that there is no sliding on the plane. μ is the dynamic friction coefficient. k_d, b_d, m_d correspond to the stiffness coefficient, the damping coefficient and the mass coefficient, respectively.

2 Aerial Manipulator Controller Design

The control of the aerial manipulator system includes the robust control of the rotorcraft and the compliance control of the manipulator. The control of the rotorcraft and the manipulator has strong force/position coupling characteristics, so the controller should have strong robustness. The control of the rotorcraft consists of a position controller and an attitude controller. According to Eq.(2), it can be seen that the position control in the x, y directions and the attitude control in the x, y directions are coupled with each other. The overall control process is shown in Fig.4. The position controller solves the desired pitch angle and roll angle, and the attitude control solves the output of the power system. The control of the manipulator adopts the admittance controller. The input of the controller is the expected contact force, so a new expected contact position is obtained and finally the admittance control is realized.

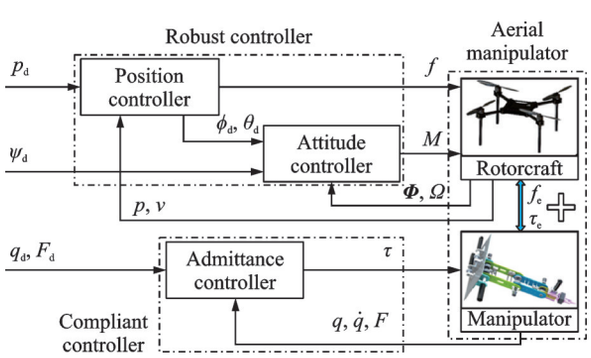

Fig.4 Control system of aerial manipulator

2.1 Rotorcraft controller design and stability analysis

The first is the design of the attitude controller. Attitude controller adopts nonsingular terminal sliding mode control based on disturbance observer. According to the dynamic equation of rotorcraft, the control of pitch angle is taken as an example, the sliding surface of the nonsingular terminal sliding mode controller is designed as

$$s_\varphi = e_\varphi + \beta \operatorname{sig}(\dot{e}_\varphi)^\alpha \tag{8}$$

where $\beta > 0$, $\operatorname{sig}(\dot{e}_\varphi)^\alpha = |\dot{e}_\varphi|^\alpha \operatorname{sign}(\dot{e}_\varphi)$; the attitude angle error of the rotorcraft is defined as $e_\varphi = \varphi_d - \varphi$.

The approximation rate of the selection is

$$\dot{s}_\varphi = -|\dot{e}_\varphi|^{\alpha-1}\left(\lambda s_\varphi + \eta \operatorname{sig}(s_\varphi)^\gamma\right) \tag{9}$$

where $\lambda > 0, \eta > 0, 0 < \gamma < 1$. The error angular acceleration and the output of the attitude controller can be obtained from Eqs.(8, 9)

$$\begin{cases} \dot{s}_\varphi = \dot{e}_\varphi + \beta\alpha|\dot{e}_\varphi|^{\alpha-1}\ddot{e}_\varphi = -|\dot{e}_\varphi|^{\alpha-1}\left(\lambda s_\varphi + \eta \operatorname{sig}(s_\varphi)^\gamma\right) \\ \ddot{e}_\varphi = -\dfrac{1}{\beta\alpha}\left(\operatorname{sig}(\dot{e}_\varphi)^{2-\alpha} + \lambda s + \eta \operatorname{sig}(s_\varphi)^\gamma\right) \\ u_2 = I_x\left[\dfrac{1}{\beta\alpha}(\operatorname{sig}(\dot{e}_x)^{2-\alpha} + \lambda s + \eta \operatorname{sig}(s_x)^\gamma) + \ddot{\varphi}_d + \dfrac{k_z}{I_x}\dot{x} - \dfrac{\tau_\varphi}{I_x} - \dot{\theta}\dot{\psi}\dfrac{(I_y - I_z)}{I_x}\right] \end{cases} \tag{10}$$

where τ_φ is the disturbance of the system, which is mainly composed of inaccurate system estimation and external disturbance. When using the approach rate of the switching property, selecting the appropriate parameters can suppress the disturbance, but at the same time cause large chattering. Therefore, this paper chooses a continuous approach rate in the boundary layer. However, when the system has uncertainty and external disturbance, the quasi-sliding mode control of the boundary layer will produce steady-state tracking error. Therefore, this paper introduces the disturbance observer to observe the noise and achieve the purpose of eliminating noise.

The design of the disturbance observer is as follows.

The auxiliary parameter L_φ is defined as

$$L_\varphi = \hat{\tau}_\varphi - KI_x\dot{\varphi} \tag{11}$$

where $\dot{\hat{\tau}}_\varphi = K(\tau_\varphi - \hat{\tau}_\varphi)$, τ_φ is the actual disturbance; $\hat{\tau}_\varphi$ the estimated observation disturbance; and $\dot{\hat{\tau}}_\varphi$ the observation error.

The derivation on both sides of the pair is

$$\dot{L}_\varphi = \dot{\hat{\tau}}_\varphi - KI_x\ddot{\varphi} \tag{12}$$

Substituting Eqs.(11, 12) into the final design of the disturbance observer is

$$\begin{cases} \dot{L}_\varphi = K(k_\varphi\dot{\varphi} - u_2 - \dot{\theta}\dot{\psi}(I_y - I_z)) - K\hat{\tau}_\varphi \\ \hat{\tau}_\varphi = L_\varphi + KI_x\dot{\varphi} \end{cases} \tag{13}$$

The design of sliding and approach rate design of the position controller are similar to those of the attitude controller. The u_1, u_{1x} and u_{1y} can be obtained, and the desired attitude angle can be obtained according to the dynamic equation.

$$\begin{cases} \phi_d = \arcsin\left(\dfrac{u_{1x}\sin\psi - u_{1y}\cos\psi}{u_1}\right) \\ \theta_d = \arcsin\left(\dfrac{u_{1x}\cos\psi + u_{1y}\sin\psi}{u_1\cos\phi}\right) \end{cases} \tag{14}$$

The stability analysis of non-singular terminal sliding mode is proved in detail in Refs.[9, 10]. Here, the stability analysis and proof of the disturbance observer are mainly given. The Lyapunov function is used to prove the stability.

The Lyapunov function of the system is

$$V = \frac{1}{2}s_\varphi^2 + \frac{1}{2}(\tilde{\tau}_\varphi)^2 \tag{15}$$

$$\begin{cases} \tilde{\tau}_\varphi = \tau_\varphi - \hat{\tau}_\varphi \\ \dot{\tilde{\tau}}_\varphi = \dot{\tau}_\varphi - \dot{\hat{\tau}}_\varphi = -\dot{\hat{\tau}}_\varphi = -K\tilde{\tau}_\varphi \end{cases} \tag{16}$$

$\dot{s}_\varphi$ calculated from Eq.(9) can be obtained

$$\dot{V} = s_\varphi\dot{s}_\varphi + \tilde{\tau}_\varphi\dot{\tilde{\tau}}_\varphi = -s_\varphi\left(\lambda s_\varphi + \eta\mathrm{sig}(s_\varphi)^\gamma\right) - K\tilde{\tau}_\varphi^2 = -\left|\dot{e}_\varphi\right|^{\alpha-1}(\lambda s_\varphi^2 + \eta s_\varphi\mathrm{sig}(s_\varphi)^\gamma) - K\tilde{\tau}_\varphi^2 \leqslant 0 \tag{17}$$

Therefore, the control system is stable.

2.2 Design of aerial manipulator admittance controller

The admittance control of the manipulator consists of two parts. The first part is the admittance controller. The input is the expected contact force and the actual contact force, and the output is the expected position error. The second part is the control of the manipulator. According to the expected position error obtained by the admittance controller, a new expected position is obtained. Then the inverse kinematics of the manipulator is solved to obtain the desired joint angle, and then the desired joint angle is Proportion integration differentiation (PID) controlled.

According to the dynamic analysis of Eq.(7), the admittance controller is designed based on the inverse kinematics as

$$\Delta x = \frac{1}{M_d s^2 + D_d s + K_d}\Delta F^{\mathrm{ext}} \tag{18}$$

Finally, the expected position deviation is output, and then the expected position is obtained. According to the expected position, the expected angle of each joint is solved by inverse kinematics. The calculation process is shown as

$$\begin{cases} q_{d2} = a\tan 2(\pm\sqrt{1-c_2^2}, c_2) \\ q_{d1} = a\tan 2(n_y, n_x) - a\tan 2(L_2 s_2, L_1 + L_2 c_2) \end{cases} \tag{19}$$

where

$$\begin{cases} n_x = P_x + \Delta x \\ n_y = P_z \\ c_2 = \dfrac{n_x^2 + n_y^2 - L_1^2 - L_2^2}{2L_1 L_2} \end{cases} \tag{20}$$

After calculating the joint angle, the PID joint angle control is carried out to output the desired joint angle acceleration. The PID angle controller is designed as

$$\alpha_d = k_p(q_d - q) + k_i\int(q_d - q) + k_d(\dot{q}_d - \dot{q}) \tag{21}$$

Finally, according to the angular acceleration, the external contact force of the manipulator is calculated, and the force/position closed-loop control is formed.

3 Control Simulation Analysis

In order to verify the effectiveness of the proposed controller, the simulation design is carried out. The parameters of the aerial manipulator are as follows. At the same time, the model estimation error is introduced to further verify the stability of the proposed controller. The actual mass of rotorcraft is m_t= 2.05 kg. The estimated mass is m=2 kg. The moment of inertia of x-y axis is I_{tx}=I_{ty}=0.125 kg·m^2. The moment of inertia of z axis is I_{tz}=0.25 kg·m^2. The estimated moment of inertia is I_x=I_y=0.13 kg·m^2,

I_z=0.24 kg·m^2, and the half of the rotor wheelbase is l=0.275 m. The mass of the arm of the manipulator is m_l=0.4 kg, in which the mass of joint 1 is m_1=0.25 kg. The mass of joint 2 is m_2= 0.15 kg, and the arm span is l_1=0.2 m, l_2=0.15 m.

In this paper, three groups of simulations are carried out. First, the control effects based on nonsingular terminal sliding mode (NTSM) and nonsingular terminal sliding mode based on disturbance observer (NTSM+DOB) are compared when the manipulator does not move (Simulation 1) and moves (Simulation 2). Second, the control effect based on NTSM+DOB when the manipulator is in contact with the outside world is carried out (Simulation 3). In addition, the system has estimation error, mechanical arm disturbance and external disturbance are considered in this system.

The parameters selected by the controllers are all the same, and the parameters of the position controller are: $\alpha=1.3$, $\beta=0.9$, $\gamma=0.8$, $[\lambda_\varphi \quad \lambda_\theta \quad \lambda_\psi]=[5 \quad 10 \quad 10]$, $[\eta_\varphi \quad \eta_\theta \quad \eta_\psi]=[10 \quad 20 \quad 20]$. Attitude controller: $\alpha=1.3$, $\beta=0.9$, $\gamma=0.8$, $[\lambda_x \quad \lambda_y \quad \lambda_z]=[5 \quad 1 \quad 1]$, $[\eta_x \quad \eta_y \quad \eta_z]=[10 \quad 5 \quad 5]$. The coefficient of the disturbance observer is K=10. Let e_{x_max}, e_{y_max} represent the maximum error in the x, y directions, respectively. And $\sqrt{e_x}$, $\sqrt{e_y}$ represent the root mean square error in the x, y direction, respectively.

Simulation 1: Figs.5, 6 show the results when the manipulator does not move. The simulation update frequency is 1 ms. The desired position of the aerial manipulator is $x_d=\sin(0.5t)$, $y_d=\sin(0.5t+\pi/2)$, $z_d=t$, and the final trajectory is a spiral.

In NTSM, e_{x_max}=107.2 mm, $\sqrt{e_x}$=20.5 mm, e_{y_max}=23 mm, $\sqrt{e_y}$=14.7 mm. There is an obvious steady-state error in the z direction due to inaccurate estimation of system parameters. The z direction can be regarded as a constant disturbance. In NTSM+DOB, e_{x_max}=106.7 mm, $\sqrt{e_x}$=19.9 mm, e_{y_max}=22.9 mm, $\sqrt{e_y}$=14.7 mm. There is no obvious steady-state error in the z direction. Therefore, it can be seen that adding a disturbance observer can eliminate the steady-state error caused by the inaccurate estimation of the system. The estimated disturbance of the disturbance observer is shown in Fig.7, and the calculated estimated value is consistent with the model inaccuracy value Δ_{mg}.

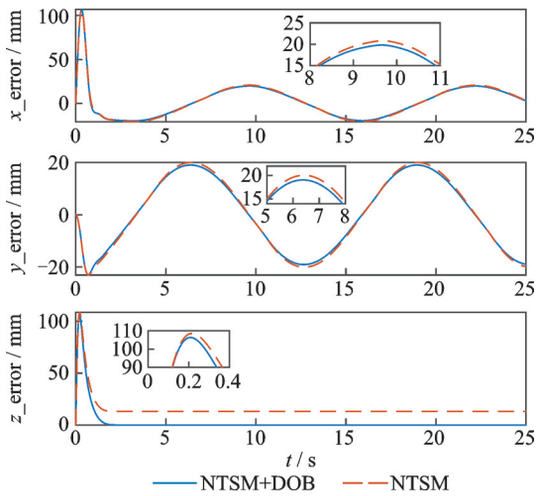

Fig.5 Comparison of Simulation 1 errors

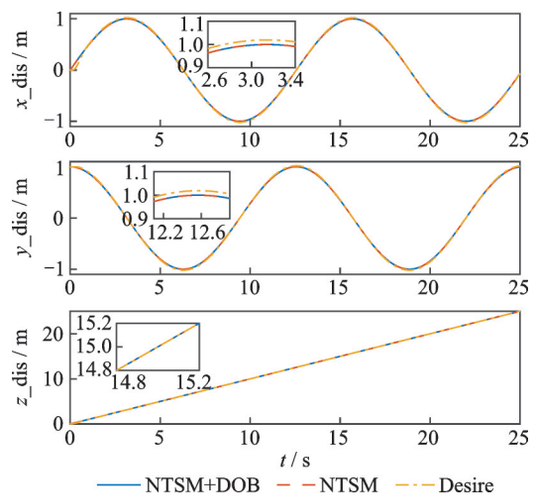

Fig.6 Trajectory comparison of Simulation 1

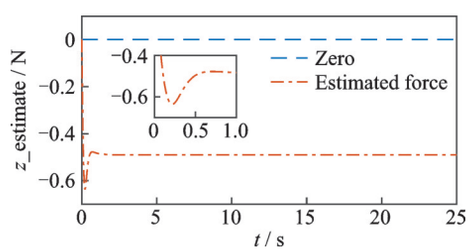

Fig.7 Observation disturbance of Simulation 1

Simulation 2: Figs.8, 9 show the results when the manipulator moves, and it is mainly the disturbance in the x-direction. The desired position of the aerial manipulator is set as $x_d=\sin(0.5t)$, $y_d=\sin(0.5t+\pi/2)$ $z_d=t$.

In NTSM, e_{x_max}=179.5 mm, $\sqrt{e_x}$=84.5 mm, e_{y_max}=144.7 mm, $\sqrt{e_y}$=29.3 mm. z di-

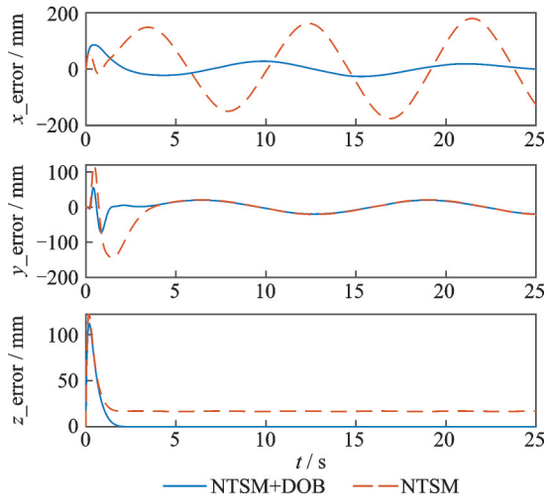

Fig.8 Comparison of Simulation 2 errors

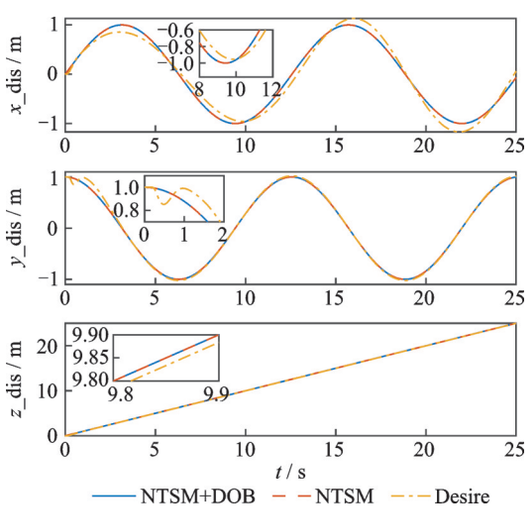

Fig.9 Trajectory comparison of Simulation 2

rection can be regarded as a constant disturbance like Simulation 1. In NTSM+DOB, $e_{x\_max}=86$ mm, $\sqrt{e_x}=27.3$ mm, $e_{y\_max}=71.7$ mm, $\sqrt{e_y}=12.8$ mm. There is no obvious steady-state error in z direction. It can be seen that the addition of the disturbance observer can greatly reduce the disturbance of the manipulator to the body.

Simulation 3: When the manipulator is in contact with the outside world, the control effect under NTSM+DOB is shown in Figs. 10, 11. At this time, the system has estimation errors, disturbances of the manipulator and external disturbances. The expected trajectory is $x_d=0$, $z_d=0$, $y_d=\sin(0.5t+\pi/2)$, the expected contact force is 4 N, so that the flying robotic arm slides on the plane with a certain contact force. It can be seen that the designed controller has good robustness and can track the expected contact force well, and finally realize the aerial contact operation of the aerial manipulator.

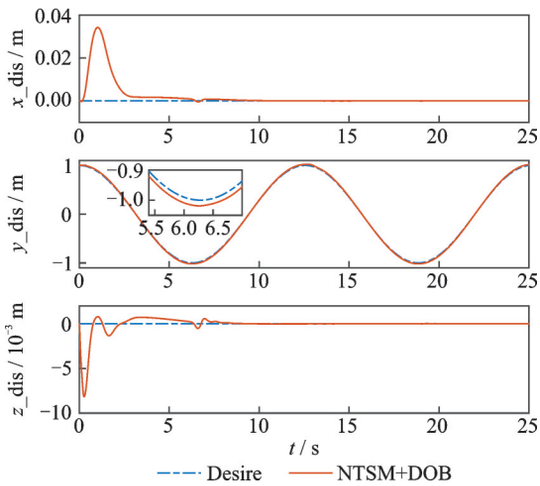

Fig.10 Trajectory of Simulation 3

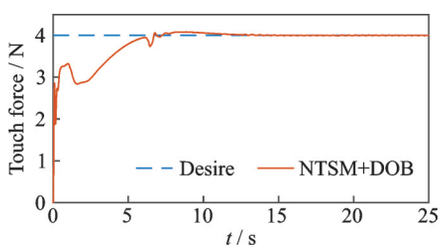

Fig.11 Expected contact force and actual force

4 Conclusions

In order to realize the contact operation of the aerial manipulator, this paper designs a cable-driven aerial manipulator, which consists of a quadrotor rotorcraft and a cable-driven manipulator. At the same time, the kinematics and dynamics analysis of the aerial manipulator and the force analysis for the contact operation scene are carried out. According to the dynamic characteristics of the aerial manipulator, a non-singular terminal sliding mode controller based on disturbance observer is designed and the stability is proved. An admittance controller is designed for the force analysis under contact operation. The simulation results show that the proposed controller has good robustness, which can reduce the system estimation error, the disturbance of the manipulator and the external disturbance, and can ensure the stability of the contact force under smooth movement.

References

[1] TAN Jianhao, WANG Yaonan, WANG Yuanyuan, et al. Research progress of rotorcraft[J]. Control Theory and Application, 2015: 1278-1286. (in Chinese)

[2] LINDSEY Q, MELLINGER D, KUMAR V. Construction of cubic structures with quadrotor teams[M]//Robotics: Science and Systems. USA: MIT Press, 2011.

[3] MENG X. Contact force control of an aerial manipulator in pressing an emergency switch process[C]//Proceedings of 2018 IEEE/RSJ International Conference on Intelligent Robots and Systems (IROS). Madrid, Spain: IEEE, 2018.

[4] BELLENS S, SCHUTTER J D, BRUYNINCKX H. A hybrid pose/wrench control framework for quadrotor helicopters[C]//Proceedings of IEEE International Conference on Robotics & Automation. Paul, USA: IEEE, 2012: 2269-2274.

[5] JAMES K, KARL S, XU W. Aerial manipulator interactions with trees for canopy sampling[J]. IEEE/ASME Transactions on Mechatronics, 2018, 23(4): 1740-1749.

[6] KIM S, SEO H, KIM H J. Operating an unknown drawer using an aerial manipulator[C]//Proceedings of IEEE International Conference on Robotics & Automation. Seattle, USA: IEEE, 2015: 5503-5508.

[7] TAKAHIRO I. Wall contact by octo-rotor UAV with one DoF manipulator for bridge inspection[C]//Proceedings of 2017 IEEE/RSJ International Conference on Intelligent Robots and Systems (IROS). Vancouver, Canada: IEEE, 2017.

[8] CACCAVALE F, GIGLIO G, MUSCIO G, et al. Cooperative impedance control for multiple UAVs with a robotic arm[C]//Proceedings of 2015 IEEE/RSJ International Conference on Intelligent Robots and Systems (IROS). Hamburg, Germany: IEEE, 2015.

[9] MENG Sihua, WANG Yaoyao, CHEN Bo, et al. Fuzzy non-singular terminal sliding mode flight control of a rope-driven flying manipulator based on time delay estimation[J]. Journal of Central South University (Natural Science Edition), 2021, 52(10): 3465-3474.

[10] YU S, YU X, SHIRINZADEH B, et al. Continuous finite-time control for robotic manipulators with terminal sliding mode[J]. Automatica, 2005, 41(11): 1957-1964.

Acknowledgement This work was supported in part by the National Natural Science Foundation of China (No. 52175097).

Authors Mr. **WEN Zunwang** received his B.S. and M.S. degrees in mechanical engineering from Nanjing University of Aeronautics and Astronautics, Nanjing, China, in 2023 and 2023, respectively. His research direction is flight robotic arm control and air ground collaboration.

Prof. **WANG Yaoyao** received his B.S. degree in mechanical engineering from Southeast University and his Ph.D. degree in mechanical engineering from Zhejiang University in 2011 and 2016, respectively. He joined the School of Mechatronics, Nanjing University of Aeronautics and Astronautics in July 2016. He mainly researches on the design, dynamics modeling and coordinated control of biomimetic aerial manipulators (BAMs), cable-driven systems (CDSs), and medical robots (MRs).

Author contributions Mr. **WEN Zunwang** completed the simulation work and main paper writing. Prof. **WANG Yaoyao** provided key guidance for the algorithm. Mr. **FU Hao** provided important suggestions for the implementation of the algorithm. Mr. **TAN Rongkai** conducted literature search and organization for the introduction of the paper, and Mr. **WANG Ning** was responsible for subsequent paper revision work. All authors commented on the manuscript draft and approved the submission

Competing interests The authors declare no competing interests.

(Production Editor: ZHANG Bei)

基于干扰估计器的飞行机械臂非奇异终端滑模柔顺控制

温尊旺，王尧尧，付　豪，谭荣凯，王　宁

(南京航空航天大学机电学院，南京 210016，中国)

摘要：针对飞行机械臂的接触作业问题，设计了一种基于干扰估计器的飞行机械臂非奇异终端滑模柔顺控制算法。该算法在非奇异终端滑模控制的基础下，引入干扰观测器，对系统的扰动进行估计，从而减小系统估计误差、机械臂的扰动以及外部扰动对飞行器的影响。最后，仿真实验结果表明，所提出的控制器具有较好的鲁棒性，可以减小系统估计误差、机械臂的扰动以及外部扰动，同时可以平稳移动下保证接触力的稳定。

关键词：飞行机械臂；干扰观测器；终端滑模；导纳控制